ACS APPLIED BIO MATERIALS

www.acsabm.org Letter

# Electrically Actuated Concentration of Microparticles through Levitation and Convective Flows in Evaporating Droplets

Anoop Menachery, Abhishek Vembadi, Ayoola Brimmo, and Mohammad A. Qasaimeh*

Cite This: https://dx.doi.org/10.1021/acsabm.0c00020 Read Online

ACCESS | Metrics & More | Article Recommendations | Supporting Information



**ABSTRACT:** We present an electrically actuated approach for creating a well-defined centered microparticle cluster within a sessile droplet on an interdigitated microelectrodes. The method is demonstrated with different aggregation shapes and particle types including biological cells for 3D microtissue development. AC voltage application induces particle levitation and enhanced-convection through accelerated evaporation. Radial long-range fluid convection evolves along the substrate surface toward the droplet's center and suspended microparticles aggregate within the central stagnation zone, in an interesting occurrence that is opposite to the well-known coffee ring effect. This remarkable approach could open new opportunities in immunoassays, rare cell counting, and 3D cell cultures.

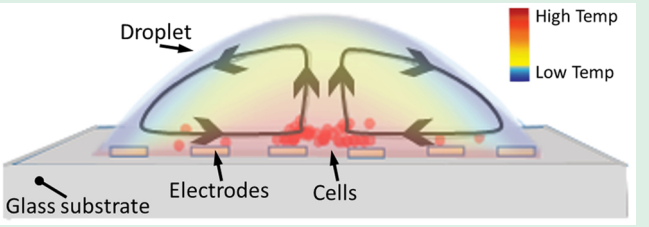


**KEYWORDS:** *microfluidics, droplet, dielectrophoresis, electrokinetics, 3D cell culture, biomaterials, microtissues*

Understanding droplet dynamics as a result of heating and evaporation is significant in many scientific disciplines and engineering applications including colloids and interfaces, microarrays, inkjet printing, and spray cooling for high power electronics.[1−3] Droplets can also be used as target carriers for biological assays, where it is employed to study probe−target interactions in proteomics and genomic research.[4] However, poor repeatability and ringlike patterns result in inconsistent spot profiles that can be rectified by utilizing precise fluid control mechanisms within these droplets.[5] A droplet on an open substrate undergoes dynamic changes commonly observed in the form of a ringlike stain when a drop of coffee dries on a surface.[6] The phenomenon was explained as an outcome of a geometrical constraint created by a pinned contact line, resulting in fluid movements to compensate for evaporative losses. Moreover, the reversal of the ringlike patterns from the periphery of the droplet to a central accumulation zone has also been reported. For example, centralized accumulation of fluorescent poly(methyl methacrylate) particles suspended within an octane droplet have been demonstrated.[7] Marangoni flow of either direction can produce deposition patterns that are central or peripheral to the drop. Another study reported the reversal of flow to produce movement of 1 $\mu$m polystyrene particles suspended in methanol/ethanol in a radially inward direction along the substrate.[3] It has been established that one can manipulate the deposition patterns and direction of flow through the alteration of the physical characteristics of the substrate and liquid.[8,9]

Previous studies have also explored the bulk movement of fluid within droplets by several means such as noncontact infrared heating of the fluid, heating of the underlying substrate, and the use of acoustic forces.[5,10,11] One approach used a laser beam to induce differential evaporation for eliminating the coffee ring effect and bringing particles, such as double stranded DNA, to the geometric center of the droplet without leaving any peripheral stains.[12] Another interesting biological application is the use of droplets for microtissue engineering to create three-dimensional multicellular clusters *in vitro* that resemble biological tissue in function. The main challenge of creating multicellular organoids using the conventional hanging drop approach is the small aggregate sizes due to the physical limitation of low droplet volumes, typically in the range 5−20 $\mu$L.[13,14] In general, understanding the contributions of certain physical phenomena within droplets such as surface tension and wettability is of significance to several fields including microfluidics, colloids, immunoassays, and biosensing.[15]

In our work, summarized in Figure 1a, electrical actuation of droplets for centralized aggregation of suspended microparticles was performed. Voltage is applied to the interdigitated microelectrodes array and the resulting electrical field within the fluid causes a dissipation of energy in the form of heat. This causes a temperature increase that leads to evaporative heat transfer and hence a thermal gradient triggered flow within the droplet. In this scenario, with a pinned contact line, the contact angle and the height of the droplet decreases, whereas the loss of liquid near the contact line is replaced by liquid from the bulk of

Received: January 8, 2020
Accepted: March 8, 2020

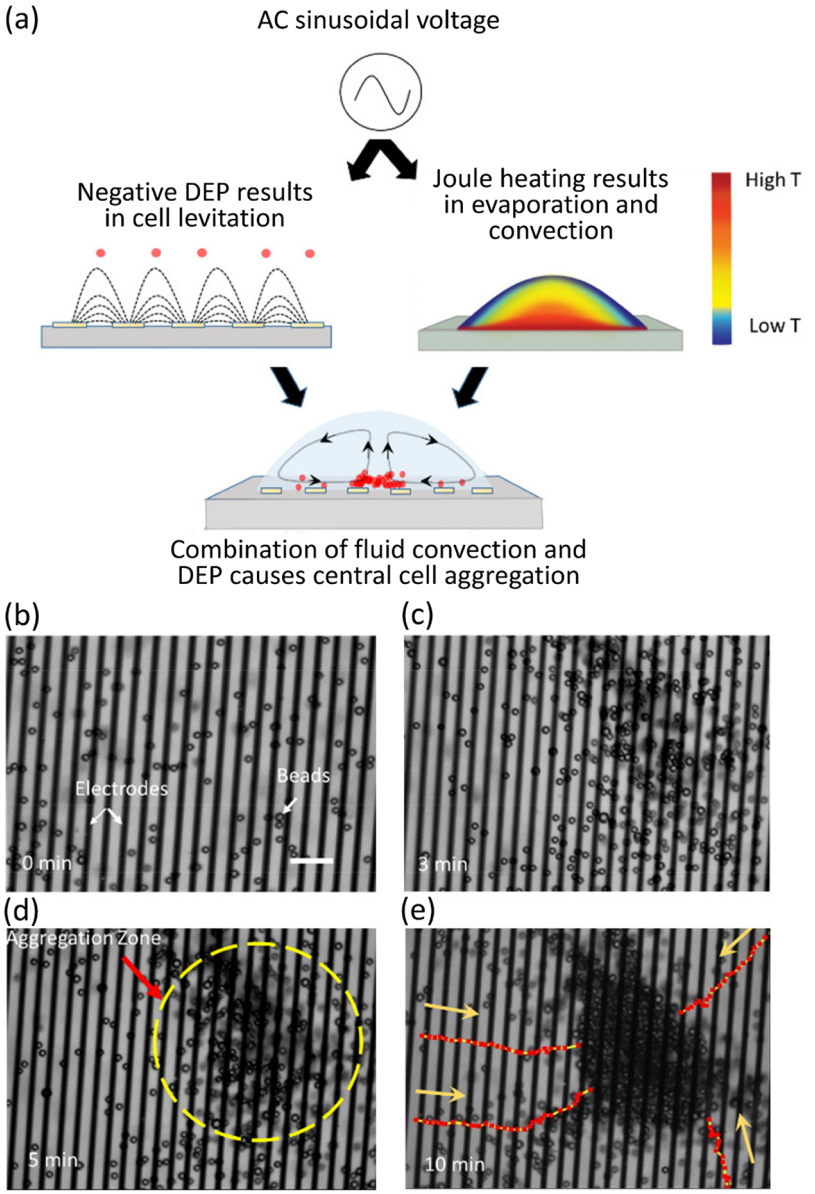


**Figure 1.** Electrically actuated concentration of microparticles within a sessile droplet placed on a substrate of interdigitated microelectrodes array. (a) Schematic of aggregating suspended particles in a droplet placed on the AC energized array. Simultaneous induction of particle levitation through negative DEP and enhanced convection through evaporation. (b)−(e) Inverted microscope images (extracted from Supplementary Video 1) of microbeads moving and aggregating in the central stagnation zone. Beads being tracked as moving into the central zone.

the droplet. We postulate that an increased evaporation rate and lower surface tension at the apex compared to the periphery results in an inward flow, down the air−liquid interface of the drop, to replenish the liquid at the contact line. Therefore, suspended microparticles flow toward the droplet's central stagnation zone, resulting in a centrally positioned aggregate. This is essentially the opposite of the coffee ring effect where a drop of the liquid dries on a surface to create a ring on the periphery of the droplet.

It is important to note that particle levitation is a key factor in this method, which prevents particles from settling on the substrate. An electrokinetic phenomenon, referred to as dielectrophoresis (DEP), is induced for particle levitation. Therefore, suspended particles flow toward the droplet's central stagnation zone, and get consequently trapped and aggregated (see Supplementary Video 1). In summary, this work presents a novel approach for centralized microparticle aggregation, generated by simultaneously triggering enhanced-convection through evaporation and negative DEP particle levitations.

The device used to generate these phenomena is a gold interdigitated microelectrodes array patterned on glass (20 $\mu$m width and spacing). It was fabricated using standard photolithography with 100 nm of gold and 5 nm of chrome, and occupy an approximate total area of 2 cm$^2$. To activate fluid flow within the 100 $\mu$L drop, a sinusoidal voltage with a frequency of 50 kHz was applied. A hydrophobic vinyl barrier was used to contain the droplet within a defined area to maintain the pinned contact line while the contact angle of the droplet decreases due to continuous accelerated evaporation.[16] The fluid flow observations were performed by using tracer beads suspended within the fluid droplet. With time, the beads gradually settled close to the electrode plane but also continued their translational radial movement toward the central aggregation zone, shown in Figure 1b−e. Progressively, the aggregate gets larger and tightly


https://dx.doi.org/10.1021/acsabm.0c00020
ACS Appl. Bio Mater. XXXX, XXX, XXX−XXX

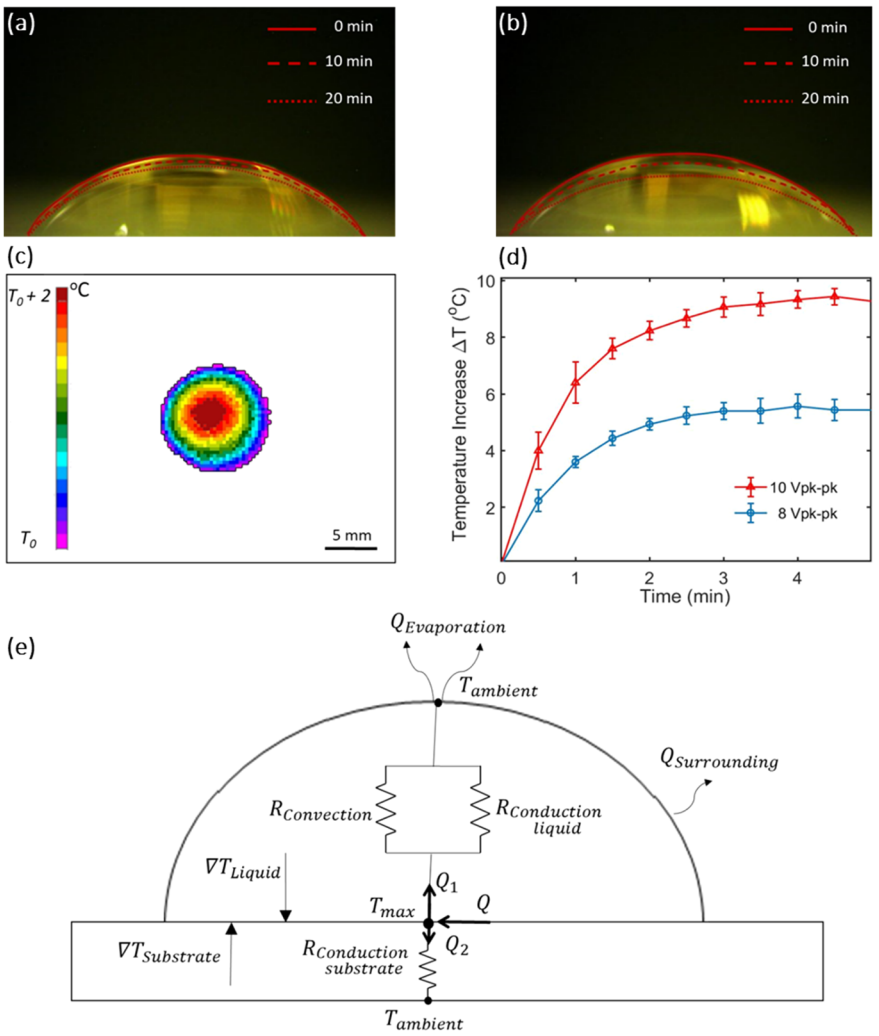


**Figure 2.** Evaporation and thermal analysis of the electrically actuated droplet. (a) Side view microscopic image of a 100 $\mu$L droplet on unenergized electrodes showing a slight reduction in volume (<5%) due to normal evaporation conditions. (b) When electrodes are energized, accelerated evaporation due to Joule heating results in a 20% reduction in droplet volume over 20 min. (c) Temperature gradient profile captured with an infrared camera mounted vertically over the droplet. The temperature increases by 2 °C from the periphery to the center of the droplet for an applied voltage of 10 $V_{pk\text{-}pk}$. This temperature gradient is maintained even as the peak temperatures at the apex and peripheral increase. (d) Temperature increase recorded between successive time points for two different voltage settings. The maximum temperature in the droplet at each time point was used to calculate $\Delta T$. Error bars indicate standard deviation of three measurements. (e) Heat transfer model for a droplet on an energized electrode surface including thermal resistances through the droplet and substrate.

packed. Some of the beads were also tracked from time-lapse microscopy images to demonstrate flow direction, as shown in Figure 1e. These images demonstrate that aggregation happens very close to the electrode plane ($Z$-direction) as the electrodes and the beads are in the same focal plane.

Evaporation of an aqueous droplet is unpreventable except if the immediate atmospheric surroundings of the vapor phase of the droplet are saturated. Our experiments were carried out in a room with controlled temperature (21 ± 1 °C) and relative humidity (~30%). However, due to the effects of Joule heating, the rate of evaporation is accelerated compared to a room temperature condition, as shown in Figure 2a,b. Joule heating occurs due to the interaction of the electrical field with an ionically conductive solution resulting in heating of the fluid. These results confirm that the droplet placed on the electrodes maintains a pinned three-phase contact line, and hence a constant footprint, throughout the period of the experiment. This also has an implication of maintaining the spherical-cap shape, as shown in Figure 2b. It is noteworthy to mention here that the shape of the droplet slightly deviates from the mathematical formulation of a spherical cap due to the effects of gravity. This does not, however, significantly impact the theoretical basis of this phenomena. The evaporative flux might vary slightly over the area of the droplet due to this shape alteration. The effects of gravity are primarily observed in the sedimentation of the beads within the convective streamlines and this remains independent of subtle variations in droplet shape.

The magnitude of the electrical field is negligible above 100 $\mu$m from the surface of the electrodes, and as a result, only a thin layer of fluid at the bottom of the droplet gets heated. However, due to the convective flows within the hemispherical droplet, a unique nonuniform temperature profile is generated. An infrared camera (FLIR T660) placed above the droplet was used to measure the spatial temperature distribution, and it was found to be warmer at the droplet apex in comparison to the periphery, by ~2 °C for 10 $V_{pk\text{-}pk}$, Figure 2c. The temperature gradually decreases toward the edge, indicating a rise of heated fluid to the


https://dx.doi.org/10.1021/acsabm.0c00020
ACS Appl. Bio Mater. XXXX, XXX, XXX−XXX

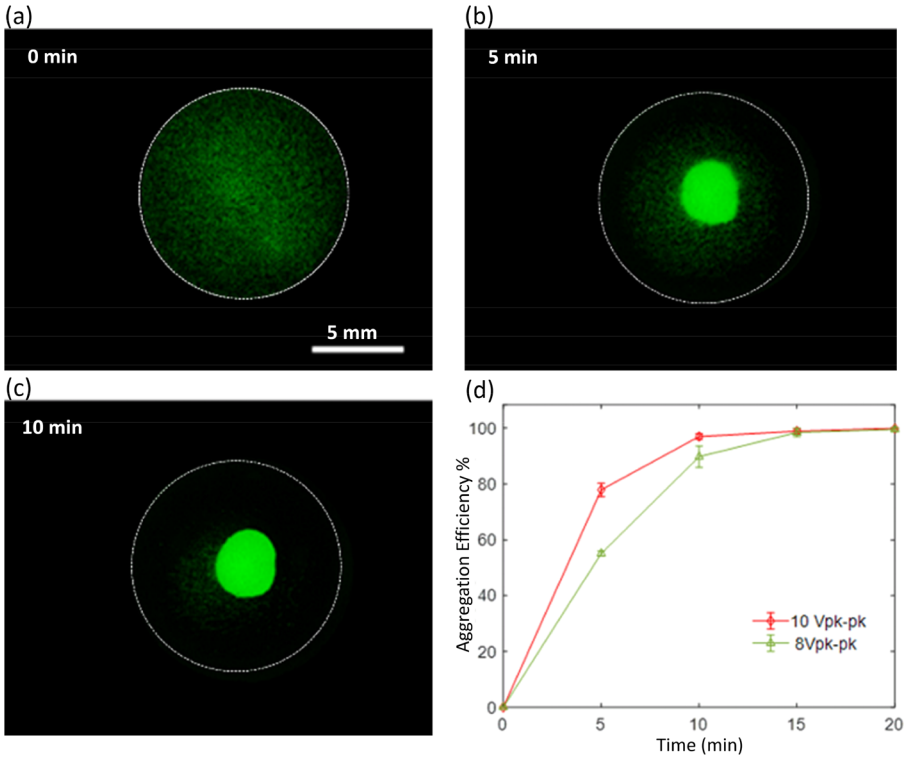


**Figure 3.** Microparticle aggregation within the electrically actuated droplet. White dotted circles represent the droplet contact line and show the constant footprint on the substrate over time. (a)−(c) Stereomicroscopic images showing a uniform suspension of fluorescent beads of 18 $\mu$m size accumulating centrally within the droplet over 10 min. (d) Aggregation efficiency obtained over time by determining the fluorescent beads that remain outside of the dense central cluster. Error bars indicate standard deviation for three independent experiments using different electrode substrates.

apex by means of convective currents. Figure 2d shows the temperature change over time for different voltages. The maximum temperature at each time point was subtracted from the ambient temperature at time zero. The temperature was recorded over a period of 5 min and was initially found to increase steeply, and eventually, a steady state temperature was reached beyond 3 min.

Heat addition by means of Joule heating is balanced by phenomena such as evaporation, convection, and conduction within the droplet and its surroundings, which results in a stabilization of temperature. The temperature at the apex of the droplet rises slower over time for 8 $V_{pk\text{-}pk}$ compared to 10 $V_{pk\text{-}pk}$ and eventually exhibits a difference of 4 °C (Figure 2d). The difference in temperature between the apex and periphery of the droplet also decreases from ∼2 to ∼1.2 °C upon lowering voltage to 8 $V_{pk\text{-}pk}$.

A heat transfer model, shown in Figure 2e, describes the heat balance for the droplet where the total power can be equated to the Joule heating term:[17]

$$Q = \sigma E^2 = Q_1 + Q_2 \tag{1}$$

where $Q$ is the total power per unit volume as a function of the electric field intensity $E$ and the ionic conductivity of the solution $\sigma$. Upon reaching steady state, the heat generated is directed upward through the liquid ($Q_1$) and down through the solid substrate ($Q_2$).

For an evaporating droplet, the power dissipated per unit volume due to evaporation can be equated to the heat conduction across the fluid ($k_l\nabla^2 T_{liq}$) and the convective component ($\rho_l c_l \mathbf{u}\cdot\nabla T_{liq}$) due to internal circulation.[18−20] The contribution due to conduction decays more rapidly with increasing height from the substrate when compared to convection due to the presence of $\nabla^2 T_{liq}$ term. Beyond a few hundred micrometers, convection is expected to dominate over conduction. Heat transfer due to evaporation is significantly higher than those due to convection and radiation at the air−liquid interface,[21] and hence $Q_{Surrounding}$ can be considered negligible. Therefore, $Q_1$ can be equated to $Q_{Evaporate}$:

$$Q_1 = \rho_l c_l \mathbf{u}\cdot\nabla T_{liq} - k_l\nabla^2 T_{liq} = Q_{Evaporate} \tag{2}$$

$$Q_{Evaporate} = \dot{m}h_{fg}/V_d \tag{3}$$

$$Q_2 = -k_s\nabla^2 T_{sub} \tag{4}$$

where $\dot{m}$ is the droplet evaporation rate, $h_{fg}$ is the latent heat of vaporization, $V_d$ is the volume of the droplet, $\rho_l$ is the density of the liquid, $c_l$ is the specific heat of the liquid, $k_l$ is the thermal conductivity of the liquid, $k_s$ is the thermal conductivity of the substrate and $\mathbf{u}$ is the average velocity of internal circulation, respectively. $\mathbf{T}_{liq}$ and $\mathbf{T}_{sub}$ denote the temperature of the liquid droplet and the temperature of the substrate, respectively.

For the sessile droplet experimented here, $T_{ambient} < T_{liq}$ and the relative humidity is 30%; therefore, the obtained evaporation rate is $\dot{m} > 0$ and $\nabla T_{liq}$ is significant, thereby driving fluid convection according to eq 2. It is important to note that these parameters are different than a typical microchannel configuration that is commonly used in electrothermal flow studies, where fluid at the top of the channel is not exposed to $T_{ambient}$, but rather a material of low thermal conductivity such as PDMS or glass. In such a scenario, the evaporation rate of $\dot{m} = 0$ and a negligible $\nabla T_{liq}$ leads to minimal heat flux through the fluid and in turn very weak convective forces. This would consequently


https://dx.doi.org/10.1021/acsabm.0c00020
ACS Appl. Bio Mater. XXXX, XXX, XXX−XXX

lead to more heat loss through the substrate into the surroundings resulting in increased $Q_2$. Hence, previously published works in the field of AC electro-hydrodynamics have not reported and described the unique observation reported in this study, which results in bulk convective flows and centralized particle aggregates.

In this setup, experimental velocity measurements were performed using an inverted microscopy setup for two voltage settings on beads that were stably suspended while simultaneously moving into the central accumulation zone. These measurements were performed using Fluoresbrite Yellow Green Microspheres with an average diameter of 18.7 $\mu$m. The conductivity of the bead suspension media ($3 \times 10^7$ bead/mL) was adjusted to 125 mS/m using phosphate buffered saline (PBS). The decrease in temperature, as a result of lowering voltage to 8 $V_{pk\text{-}pk}$, reduces velocity by ~3 $\mu$m/s from an average value of ~15 $\mu$m/s at 10 $V_{pk\text{-}pk}$. As a result, the decrease in velocity causes a change in aggregation rate of the microparticles.

Aggregation efficiency is defined as the percentage of beads within the cluster, which increases over time corresponding to a decreasing fluorescent bead intensity in the medium surrounding the cluster. Figure 3a was obtained using an SMZ18 stereomicroscope to study the gradual accumulation of beads at the center of the droplet over time. The accumulation efficiency was calculated for time-lapse images based on the difference in intensity between the initial suspension and the central bead aggregate. Image segmentation using Icy and ImageJ were implemented for active edge detection based on intensity thresholding to identify and locate the central accumulation region. The decrease of voltage from 10 to 8 $V_{pk\text{-}pk}$ results in approximately 20% lower aggregation efficiency at 5 min (Figure 3b). However, as the experiment progresses, differences in bead aggregation observed between voltages diminishes and efficiencies reach a maximum of 99%. The rate of aggregation is initially steeper due to higher bead amounts present directly above the aggregation zone in the spherical-cap shaped droplet. In this geometry, the volume of fluid contained directly above the substrate is highest within the central region and decreases sharply toward the periphery. In addition, beads that are initially suspended further away from the central region, take longer to arrive at the central aggregation zone because they need to traverse a longer distance along the substrate once they reach a stable levitation height. Hence, aggregation efficiency is significantly higher during the first 5 min and sharply reduces toward the end of the experiment (Figure 3b).

The results clearly indicate that the fluid movement is actuated by a temperature gradient. Evaporation is considered to be the primary process influencing convection within the droplet, and this was established by performing control experiments where the immediate environment around the droplet was saturated by the water vapor phase. This was performed by placing an energized electrode substrate within a water bath with a relative humidity measured at over 90%, and hence the effects of evaporation can be considered negligible. In this configuration, we did not observe any accumulation in the center after 20 min of actuating the electrodes, Supplementary Figure S1. This leads us to conclude that capillary flow due to evaporation is mainly responsible for the observed phenomenon. It is also necessary to establish why the capillary flow direction is radially inward along the substrate surface. To understand this further, it will be beneficial to compare the method employed in our studies with a conventional coffee-ring phenomenon,[22] where the droplet is placed on a heated substrate. The experimentally measured temperature profiles of droplets on a heated substrate, especially metal substrates with very high thermal conductivity, indicate a cooler temperature at the apex of the droplet compared to the periphery which is hotter.[10] For a droplet on a heated substrate, the cumulative effects of convective heat transfer through the surrounding air and radiation results in the periphery of the drop to maintain a higher temperature than the apex of the drop. In such a setup, the top of the droplet is colder than the bottom due to the increased conduction path from the heated substrate, resulting in increased evaporation at the periphery of the pinned droplet compared to the apex, causing flow that is directed radially outward. In our setup, the convection current is reversed, causing flow that is directed radially inward to the center of the drop despite the effects of Joule heating taking place at the bottom of the substrate. This is because the substrate used here is a very thin (100 nm thick) patterned film of gold on glass, where glass has a low thermal conductivity approximately the same as the water droplet. This will result in little heat transfer from the fluid to the glass maintaining the glass substrate at a lower temperature than the fluid undergoing Joule heating at the bottom of the droplet. Therefore, with a stable radially inward convective pattern, we are able to achieve a temperature profile where the apex can be maintained at a higher temperature by means of convection. In addition to capillary flow caused by evaporation, temperature gradients over the droplet surface also produce differences in the surface tension that lead to Marangoni flow. Surface tension is higher in the colder regions, which in our experiments correspond to the periphery of the drop along the air−liquid interface, shown in Figure 2c. Hence, the fluid flow due to the Marangoni effect is in the same radial inward direction as the capillary flow caused due to evaporation. The exact contribution of Marangoni flow is difficult to estimate, but in smaller droplets, it is generally understood that the Marangoni convection is more dominant than buoyant convection. For an aqueous droplet, the transition from Marangoni toward buoyancy driven flow occurs when the characteristic length is greater than 1 cm,[23] which is not the case in this work. Experimental evaluation of the circulating convective fluid flow pattern was performed using 6 $\mu$m fluorescent beads to further substantiate the phenomena (Supplementary Figure S2 and Supplementary Video 2). It clearly demonstrates the 6 $\mu$m beads moving up from the stagnation zone at the center of the droplet. From the apex, where the temperature is higher, the beads are observed moving toward the periphery along the liquid−air interface and then radially inward back to the center of the droplet.

In electrically charged fluid, it is also essential to consider the influence of other electro-hydrodynamic phenomena within our experiments. Two commonly reported phenomena are electrothermal flow and AC electroosmotic flow.[24] In the case of AC electroosmosis, a force on the ions in the electrical double layer leads to fluid motion close to the electrode edges causing microparticle accumulation at each electrode within the array, unlike a centralized pattern observed in our experiments. Additionally, suspending medium conductivities of 125 mS/m should exhibit extremely weak flows, and hence the effects of AC electroosmosis can be considered negligible. In the case of electrothermal flow, Joule heating gives rise to conductivity and permittivity gradients within the suspending medium, resulting in an electrical body force driving fluid flow. The force decreases significantly with decaying electric field strengths, and hence


https://dx.doi.org/10.1021/acsabm.0c00020
ACS Appl. Bio Mater. XXXX, XXX, XXX−XXX

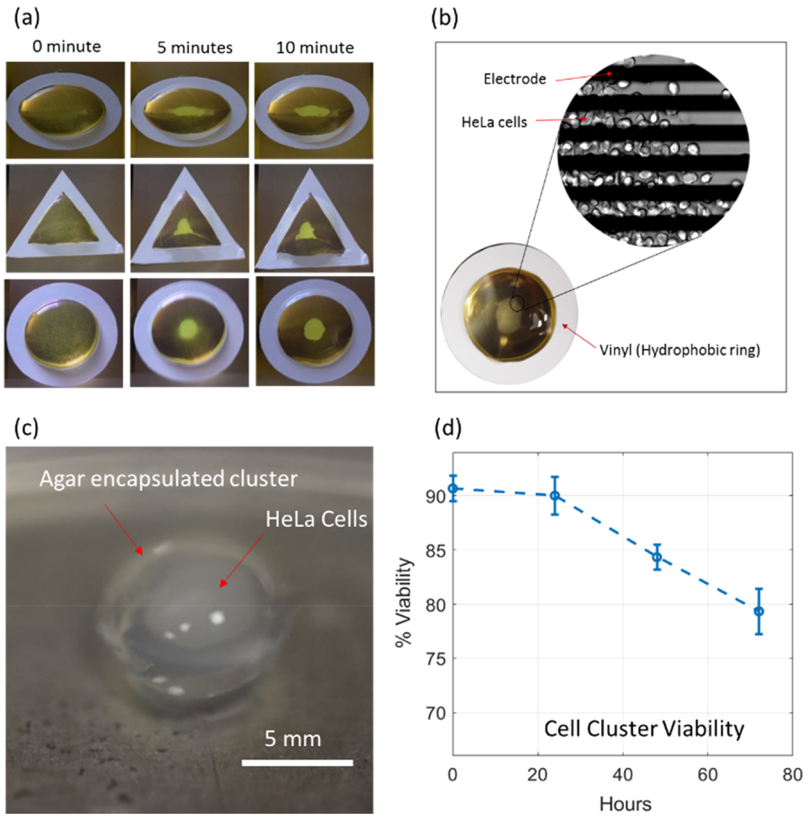


**Figure 4.** Versatility and robustness of the method to achieve aggregation of different shapes and particle types. (a) Oval, triangular, and circular vinyl hydrophobic barriers result in aggregation patterns that mimic the shape of the droplet. (b) HeLa cells were used to demonstrate that biological particles achieve similar dense aggregates using this technique signifying wide applicability of the approach. (c) The dense HeLa cell aggregate was encapsulated with agar and moved to a regular culture plate to form a 3D cell culture. (d) Viability of the cellular aggregates over time was determined using a live/dead assay.

within our droplets, which have a height in the order of millimeters, it is unlikely to be a major contributing factor.

Levitation is necessary to keep particles suspended in the fluid without settling on the bottom electrode substrate, and this is achieved by means of DEP. DEP results in the movement of particles experiencing a nonuniform electric field, typically toward the electrode edges in the case of positive DEP and away from the electrodes in the case of negative DEP.[25] When 18 $\mu$m polystyrene beads are suspended in a 125 mS/m aqueous solution, a negative DEP force dominates a large portion of the AC frequency spectrum from 10 kHz to 10 MHz. Here, the microelectrodes were energized with a sinusoidal voltage of 10 $V_{pk\text{-}pk}$ with a frequency of 50 kHz, which results in particles moving away from the high field regions toward low electric field intensity areas. For the 20 $\mu$m interdigitated electrodes, negative DEP results in levitation of the particles above the electrode plane, typically to a height of 20−60 $\mu$m. This prevents the microparticles from settling and enabling them to be carried along with the flow into the bottom center of the droplet. It stays at the geometric center and does not get carried along with the convective flows upward because the velocity is insufficient in that stagnation region to overcome gravitational forces. Hence, the condition for controlled levitation and aggregation at the substrate surface is when $\vec{F}_{DEP}$ balances the gravitational component ($\vec{F}_g$), and the drag force is negligible in the bottom center "stagnation zone" of the droplet.

$$\vec{F}_{DEP} = \vec{F}_g \quad \text{and} \quad 6\pi\eta r(\vec{V}) \approx 0 \tag{5}$$

Interdigitated electrodes have been used for particle levitation, where levitation height can be determined as[26]

$$h = \frac{d}{\pi} \ln\left[-\frac{24V_0^2\varepsilon_m \mathrm{Re[CM]}}{4d^3(\rho_p - \rho_m)g}\right] \tag{6}$$

The voltage used was 10 $V_{pk\text{-}pk}$ on an interdigitated electrode with a gap ($d$) of 20 $\mu$m. The real part of the Clausius−Mossotti factor (Re[CM]) is −0.5. The density of the polystyrene bead and the cells was assumed to be 1055 kg/m$^3$. The density of the suspending medium containing 10% sucrose is approximately 1038 kg/m$^3$, whereas the density will be approximately 1000 kg/m$^3$ when the medium does not contain sucrose. $\varepsilon_m$ is the absolute permittivity of the suspending medium, which valued as $710 \times 10^{-12}$ (F/m).

In order to experimentally measure the levitation height of the beads, an interdigitated electrode chip was mounted on the inverted microscope. A suspension of 18 $\mu$m beads in the DEP buffer was introduced onto the surface of the energized electrodes. The electrode surface was visually observed on a lower focal plane from the levitated beads. Along with levitation, the beads simultaneously underwent X−Y translational movement into the center of the droplet. By turning the focus knob on the microscope, vertical movement of the objective and the corresponding change in the focal point were used to carry out levitation height measurements. By precisely measuring the knob rotation within the electrode and beads focal plane (Supplementary Figure S3), we were able to estimate the height of the beads above the surface of the electrodes. On the basis of


https://dx.doi.org/10.1021/acsabm.0c00020
ACS Appl. Bio Mater. XXXX, XXX, XXX−XXX

10 measurements, we estimated the levitation height as 24.4 ± 4.1 $\mu$m. However, using eq 6, the levitation height is expected to be around 60 $\mu$m when the buffer contains 8.5% sucrose. We postulate that this discrepancy could be attributed to two factors, namely, electrode polarization effects and slightly downward pointing fluid flow vectors. Electrode polarization would effectively lower the net voltage for levitation and Joule heating due to an electrical double layer on the electrode surface and its effect on applied voltage has been previously explored.[27] In addition to this, the fluid velocity vector close to the electrode surface could have a downward component that would counter the stationary DEP levitation forces, thereby effectively reducing the net levitation height predicted from the theoretical formulation provided here. Other factors contributing to this variation could also include variability in bead size, the density of beads, and density of the fluid medium.

The discussed phenomenon and apparatus in this work is extremely versatile given its capability to accommodate different particles such as biological cells, and it can also be used to generate aggregates of various shapes resembling the outline of the fluid droplet. Three hydrophobic barriers were used to contain fluid within oval, triangular, and circular shapes, to demonstrate that the clusters mirror the geometry of the droplet as shown in Figure 4a. The flow pattern generated within the droplet is symmetrical about the center of the droplet, resulting in particle accumulation at that point. As an example, the temporal evolution of the triangular aggregate starts with the beads forming arms from the center and extending toward the vertices. These arms subsequently get shorter and wider over time and eventually withdraw to create a centered triangular cluster.

Beads were substituted with HeLa cancer cells to show particles with different composition can also be used to achieve similar aggregation. HeLa cancer cells were washed and suspended in an isotonic, pH adjusted 125 mS/m conductivity media containing 8.5% sucrose and 0.3% dextrose, which is essential to maintain cell viability. Despite the resulting change in medium properties, such as density, viscosity, and surface tension, the observed fluid convection phenomenon is still efficacious to produce dense clusters as shown in Figure 4b. For 3D cell culture applications, we devised a process of creating microtissues by the addition of 0.2% low temperature gelling agar to the cell suspension in DEP buffer media and by placing the electrode substrate on a warm metal block to maintain lower fluid viscosity. Once the cluster was formed with this convective phenomenon, the 0.2% liquid agar solution was gelled by placing the metal block with the electrode substrate in an ice bucket. To further fortify the gelled cellular cluster, an additional 80 $\mu$L of 1% agar is added over the sessile droplet. This enables the gelled cluster to be transferred into cell culture media for continued cell proliferation and viability studies, as shown in Figure 4c. Cell viability studies on the encapsulated cluster were performed using a live/dead cytotoxicity assay containing Calcein AM and Ethidium Homodimer. The fluorescent signal was observed using FITC and TRITC filters, and a very low but uniform distribution of dead cells was observed evenly through the cluster. The viability over a 72 h period was found to be within standard values reported in the literature, as shown in Figure 4d. To demonstrate diversity of the method for mammalian cells, the experiment was repeated with T-lymphocytes (approximately 10 $\mu$m in diameter). Results showed similar accumulation patterns (Supplementary Figure S4). The robustness of the method for creating well-defined 3D microtissues in an *in vitro* environment holds exciting applications in engineering of biopatterned tissues. Several studies have explored methods for bio-microfabrication of cells integrated within gel substrates.[28,29] Our method can be replicated for developing heterogeneous microtissues consisting of two different kinds of cells arranged in various shapes and sizes in an extracellular matrix.[30] Furthermore, in future experiments, the microtissues can be arranged in arrays on a chip for high throughput drug screening applications.

In conclusion, we present a novel and simple electrically triggered method driven by accelerated evaporation for achieving central microparticles aggregation. A droplet of 100 $\mu$L used in our experiments maintains a spherical-cap shape, and when it is subjected to increased evaporative flux, liquid is replenished by means of circulation to keep the droplet's contact line pinned. This is the first detailed study that incorporates the use of microelectrodes to trigger bulk volumetric flow within the droplet to achieve a defined central aggregation pattern. The adopted approach works even when the suspending fluid is altered by the addition of a solute such as sucrose and agar. This clearly demonstrates the applicability of this technique for use in biology where the medium composition must contain a high solute concentration. The robustness of this technique is proven by the aggregation of particles in various shape configurations due to its ability to generate symmetrical flow about a central stagnation zone. This work provides a unique platform that can be used for biological applications such as microtissue engineering. Future applications may involve developing ultrasensitive immunoassays powered with the enhanced mass transport, extremely low concentration cell counters including circulating tumor cells, and automated high-throughput platforms for constructing 3D cell microcultures with different shapes and sizes.

## ■ ASSOCIATED CONTENT

### Supporting Information

The Supporting Information is available free of charge at https://pubs.acs.org/doi/10.1021/acsabm.0c00020.

Figure S1, stereomicroscopic images showing a uniform suspension of fluorescent beads at 90% relative humidity; Figure S2, horizontal microscopic image showing the convective flow pattern using fluorescent beads; Figure S3, microscopic images showing bead levitation due to the negative DEP forces; Figure S4, central aggregate formation of T-cell suspension in buffer (PDF)

Video of beads accumulation at the droplet's central stagnation zone (MP4)

Side-view video of a droplet showing the convective flow pattern using fluorescent beads (MP4)

## ■ AUTHOR INFORMATION

### Corresponding Author

**Mohammad A. Qasaimeh** − *Division of Engineering, New York University Abu Dhabi, Abu Dhabi, UAE; Department of Mechanical and Aerospace Engineering, Tandon School of Engineering, New York University, Brooklyn, New York 11201, United States;* orcid.org/0000-0003-1122-9698; Email: maq4@nyu.edu

### Authors

**Anoop Menachery** − *Division of Engineering, New York University Abu Dhabi, Abu Dhabi, UAE*



https://dx.doi.org/10.1021/acsabm.0c00020
ACS Appl. Bio Mater. XXXX, XXX, XXX−XXX

**Abhishek Vembadi** − *Division of Engineering, New York University Abu Dhabi, Abu Dhabi, UAE*

**Ayoola Brimmo** − *Division of Engineering, New York University Abu Dhabi, Abu Dhabi, UAE; Department of Mechanical and Aerospace Engineering, Tandon School of Engineering, New York University, Brooklyn, New York 11201, United States*

Complete contact information is available at: https://pubs.acs.org/10.1021/acsabm.0c00020

### Notes

The authors declare no competing financial interest.

## ■ ACKNOWLEDGMENTS

This work was supported by Seed Grants (AJF201523 and AJF2018085) from Al Jalila Foundation, Dubai, UAE, the ADEK Award for Research Excellence (AARE-2015), Abu Dhabi Department of Education and Knowledge, Abu Dhabi, UAE, and New York University Abu Dhabi. We acknowledge the technical assistance from Dr. Muhammedin Deliorman and technical support from the Core Technology Platforms at NYU Abu Dhabi.

## ■ REFERENCES

(1) Derby, B. Additive manufacture of ceramics components by inkjet printing. *Engineering* **2015**, *1* (1), 113−123.

(2) Handscomb, C.; Kraft, M.; Bayly, A. A new model for the drying of droplets containing suspended solids. *Chem. Eng. Sci.* **2009**, *64* (4), 628−637.

(3) Ristenpart, W.; Kim, P.; Domingues, C.; Wan, J.; Stone, H. A. Influence of substrate conductivity on circulation reversal in evaporating drops. *Phys. Rev. Lett.* **2007**, *99* (23), 234502.

(4) Dixit, C.; Aguirre, G. Protein microarrays with novel microfluidic methods: current advances. *Microarrays* **2014**, *3* (3), 180−202.

(5) Girard, F.; Antoni, M. Influence of substrate heating on the evaporation dynamics of pinned water droplets. *Langmuir* **2008**, *24* (20), 11342−11345.

(6) Deegan, R. D.; Bakajin, O.; Dupont, T. F.; Huber, G.; Nagel, S. R.; Witten, T. A. Capillary flow as the cause of ring stains from dried liquid drops. *Nature* **1997**, *389* (6653), 827.

(7) Hu, H.; Larson, R. G. Marangoni effect reverses coffee-ring depositions. *J. Phys. Chem. B* **2006**, *110* (14), 7090−7094.

(8) Chen, X.; Wang, X.; Chen, P. G.; Liu, Q. Thermal effects of substrate on Marangoni flow in droplet evaporation: response surface and sensitivity analysis. *Int. J. Heat Mass Transfer* **2017**, *113*, 354−365.

(9) Yu, Y.-S.; Wang, M.-C.; Huang, X. Evaporative deposition of polystyrene microparticles on PDMS surface. *Sci. Rep.* **2017**, *7* (1), 14118.

(10) Girard, F.; Antoni, M. l.; Sefiane, K. Infrared thermography investigation of an evaporating sessile water droplet on heated substrates. *Langmuir* **2010**, *26* (7), 4576−4580.

(11) Reboud, J.; Bourquin, Y.; Wilson, R.; Pall, G. S.; Jiwaji, M.; Pitt, A. R.; Graham, A.; Waters, A. P.; Cooper, J. M. Shaping acoustic fields as a toolset for microfluidic manipulations in diagnostic technologies. *Proc. Natl. Acad. Sci. U. S. A.* **2012**, *109* (38), 15162−15167.

(12) Yen, T. M.; Fu, X.; Wei, T.; Nayak, R. U.; Shi, Y.; Lo, Y.-H. Reversing Coffee-Ring Effect by Laser-Induced Differential Evaporation. *Sci. Rep.* **2018**, *8* (1), 3157.

(13) Foty, R. A simple hanging drop cell culture protocol for generation of 3D spheroids. *J. Visualized Exp.* **2011**, No. 51, No. e2720.

(14) Timmins, N. E.; Nielsen, L. K. Generation of Multicellular Tumor Spheroids by the Hanging-Drop Method. In *Tissue Engineering*; Hauser, H., Fussenegger, M., Eds.; Humana Press: Totowa, NJ, 2007; pp 141−151.

(15) He, B.; Yang, S.; Qin, Z.; Wen, B.; Zhang, C. The roles of wettability and surface tension in droplet formation during inkjet printing. *Sci. Rep.* **2017**, *7* (1), 11841.

(16) Wang, F.-C.; Wu, H.-A. Pinning and depinning mechanism of the contact line during evaporation of nano-droplets sessile on textured surfaces. *Soft Matter* **2013**, *9* (24), 5703−5709.

(17) Kim, Y. C. Evaporation of nanofluid droplet on heated surface. *Adv. Mech. Eng.* **2015**, *7* (4). DOI: 10.1177/1687814015578358

(18) Mandal, D. K.; Bakshi, S. Internal circulation in a single droplet evaporating in a closed chamber. *Int. J. Multiphase Flow* **2012**, *42*, 42−51.

(19) Morgan, H.; Green, N. *AC electrokinetics: colloids and nanoparticles*; Research Studies Press Ltd.: Baldock, England, 2003.

(20) Jaiswal, V.; Harikrishnan, A. R.; Khurana, G.; Dhar, P. Ionic solubility and solutal advection governed augmented evaporation kinetics of salt solution pendant droplets. *Phys. Fluids* **2018**, *30* (1), 012113.

(21) Bergman, T. L.; Lavine, A. S.; Incropera, F. P.; DeWitt, D. P. *Fundamenals of heat and mass transfer*. 8th ed.; Wiley, 2010.

(22) Lama, H.; Basavaraj, M. G.; Satapathy, D. K. Tailoring crack morphology in coffee-ring deposits via substrate heating. *Soft Matter* **2017**, *13* (32), 5445−5452.

(23) Tam, D.; von ARNIM, V.; McKinley, G.; Hosoi, A. Marangoni convection in droplets on superhydrophobic surfaces. *J. Fluid Mech.* **2009**, *624*, 101−123.

(24) García-Sánchez, P.; Ramos, A. AC Electroosmosis: Basics and Lab-on-a-Chip Applications. *Encyclopedia of Nanotechnology* **2015**, 33−39.

(25) Castellanos, A.; Ramos, A.; Gonzalez, A.; Green, N. G.; Morgan, H. Electrohydrodynamics and dielectrophoresis in microsystems: scaling laws. *J. Phys. D: Appl. Phys.* **2003**, *36* (20), 2584.

(26) Morgan, H.; Izquierdo, A. G.; Bakewell, D.; Green, N. G.; Ramos, A. The dielectrophoretic and travelling wave forces generated by interdigitated electrode arrays: analytical solution using Fourier series. *J. Phys. D: Appl. Phys.* **2001**, *34* (10), 1553.

(27) Markx, G.; Pethig, R.; Rousselet, J. The dielectrophoretic levitation of latex beads, with reference to field-flow fractionation. *J. Phys. D: Appl. Phys.* **1997**, *30*, 2470.

(28) Li, Y.; Yan, X.; Liu, W.; Zhou, L.; You, Z. Du. 3D microtissues for injectable regenerative therapy and high-throughput drug screening. *J. Visualized Exp.* **2017**, *128*, 55982.

(29) Lee, G. G.; Lee, J. S.; Wang, X.; Lee, S. H. Bottom up engineering of well defined 3D microtissues using microplatforms and biomedical applications. *Adv. Healthcare Mater.* **2016**, *5*, 56.

(30) Menachery, A.; Vembadi, A.; Sukumar, P.; Rezgui, R.; Qasaimeh, M. A. Rapid and spatially separated heterogeneous 3D cellular patterning using electrohydrodynamics. In *Proceedings of the 23rd International Conference on Miniaturized Systems Chemistry Life Sciences*, Basel, Switzerland, 2019; pp 334−335.

# Supporting Information

## Electrically Actuated Concentration of Microparticles through Levitation and Convective Flows in Evaporating Droplets

Anoop Menachery [a], Abhishek Vembadi [a], Ayoola Brimmo [a,b], and Mohammad A. Qasaimeh [a,b] *

[a] Division of Engineering, New York University Abu Dhabi, UAE.

[b] Department of Mechanical and Aerospace Engineering, Tandon School of Engineering, New York University, 6 Metrotech Center, Brooklyn, NY 11201, USA.

***Email: maq4@nyu.edu**

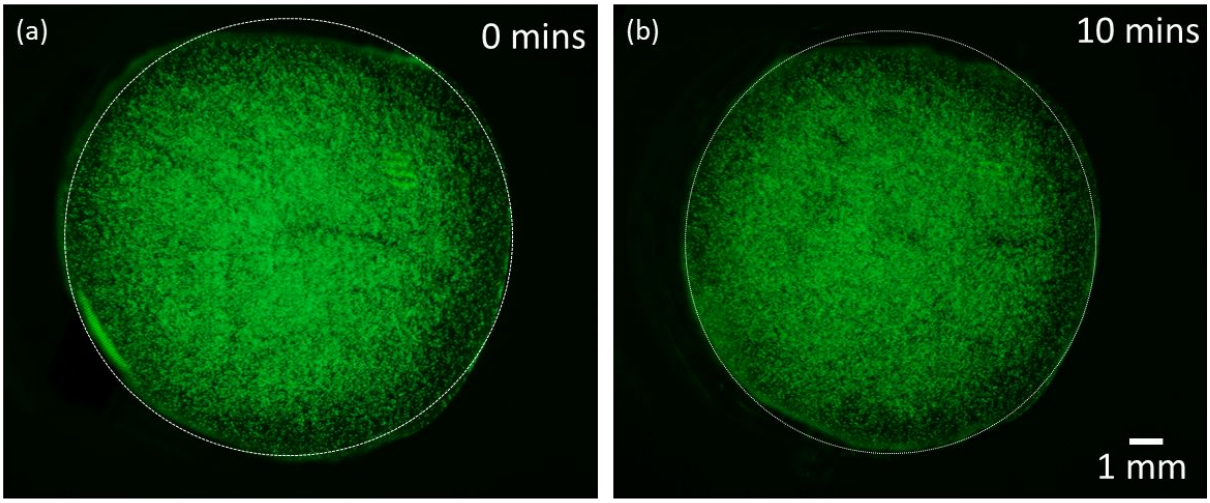


Figure S1: Stereomicroscopic images showing a uniform suspension of fluorescent beads of 18 μm size at 90% relative humidity. White doted circles represent the droplet contact line and show the constant footprint on the substrate over time. (a) The uniform suspension of beads before energizing the interdigitated microelectrodes array. (b) The suspension of beads remains uniform after energizing the array for 10 minutes. At 90% relative humidity, evaporation is negligible and hence the phenomenon is not triggered, where no central aggregation is observed.

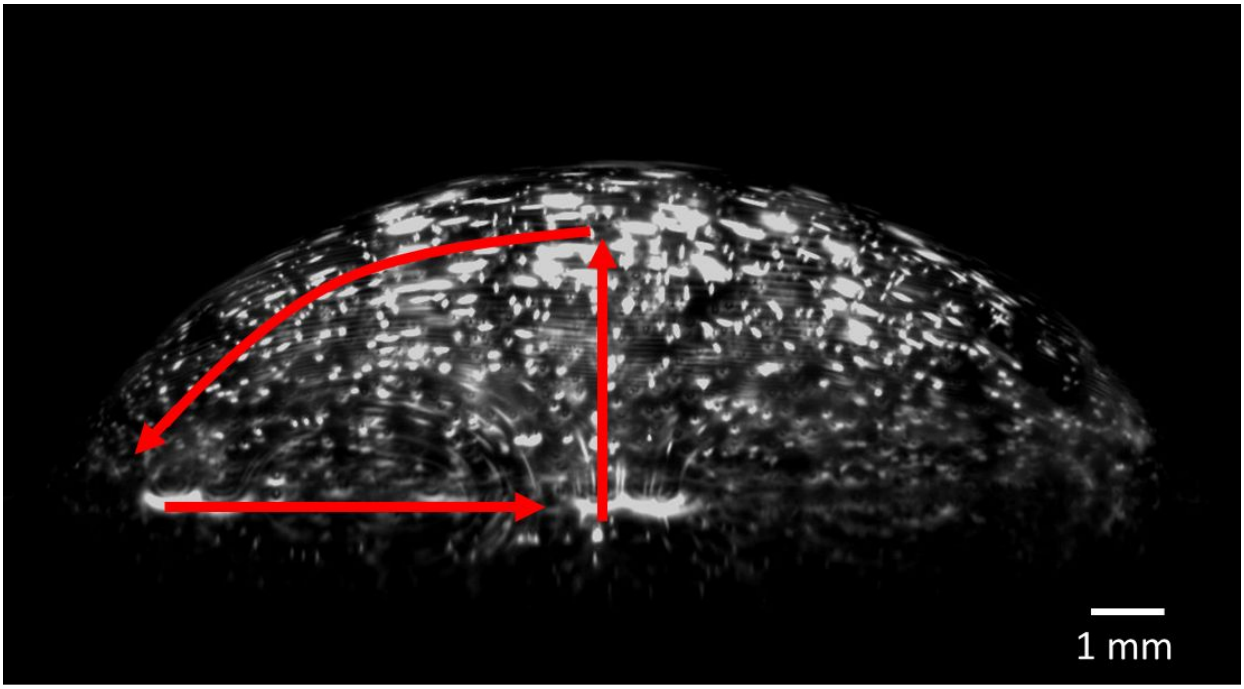


Figure S1: Horizontal microscopic image showing the convective flow pattern using fluorescent 6 μm beads. The high apex temperature causes the fluid to rise above from the stagnation point at the center of the droplet. The fluid then flows to periphery of the droplet along the liquid-air interface due to capillary flow and then it follows radially inward to the center of the droplet. This continuous and symmetrical fluid circulation is observed in entire 3-dimensional space within the droplet. Refer to Supplementary Video 2.

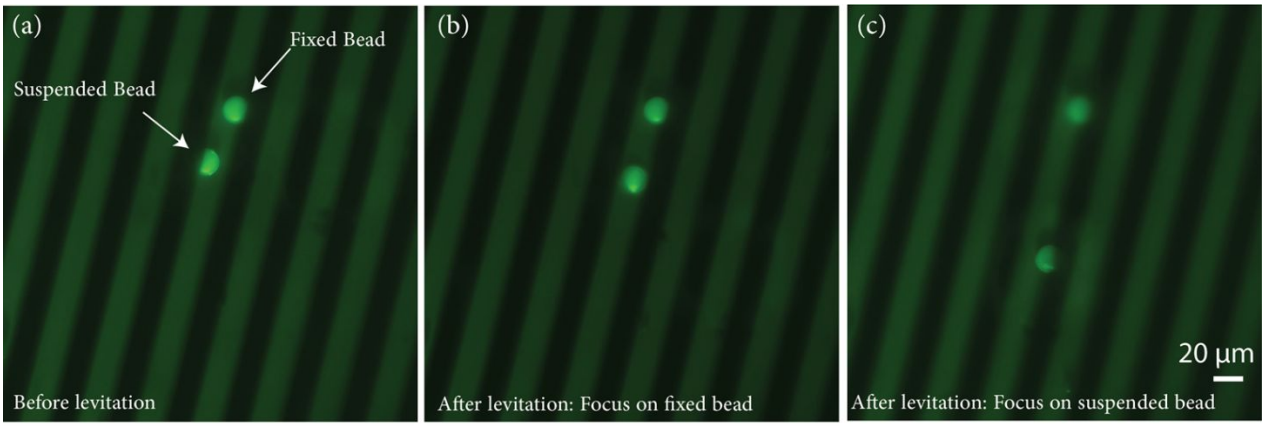


Figure S3: Microscopic images describing the methodology for measuring the levitation height of suspended bead. (a) Before introduction of DEP forces. The suspended bead, fixed bead (height reference), and electrodes are all in focus. (b) Immediately after introduction of DEP forces. The suspended bead levitates to go out of focus while electrodes and the fixed bead remain in focus. (c) After introduction of DEP forces and refocusing camera on the levitated bead. Fixed bead and electrodes are out of focus.

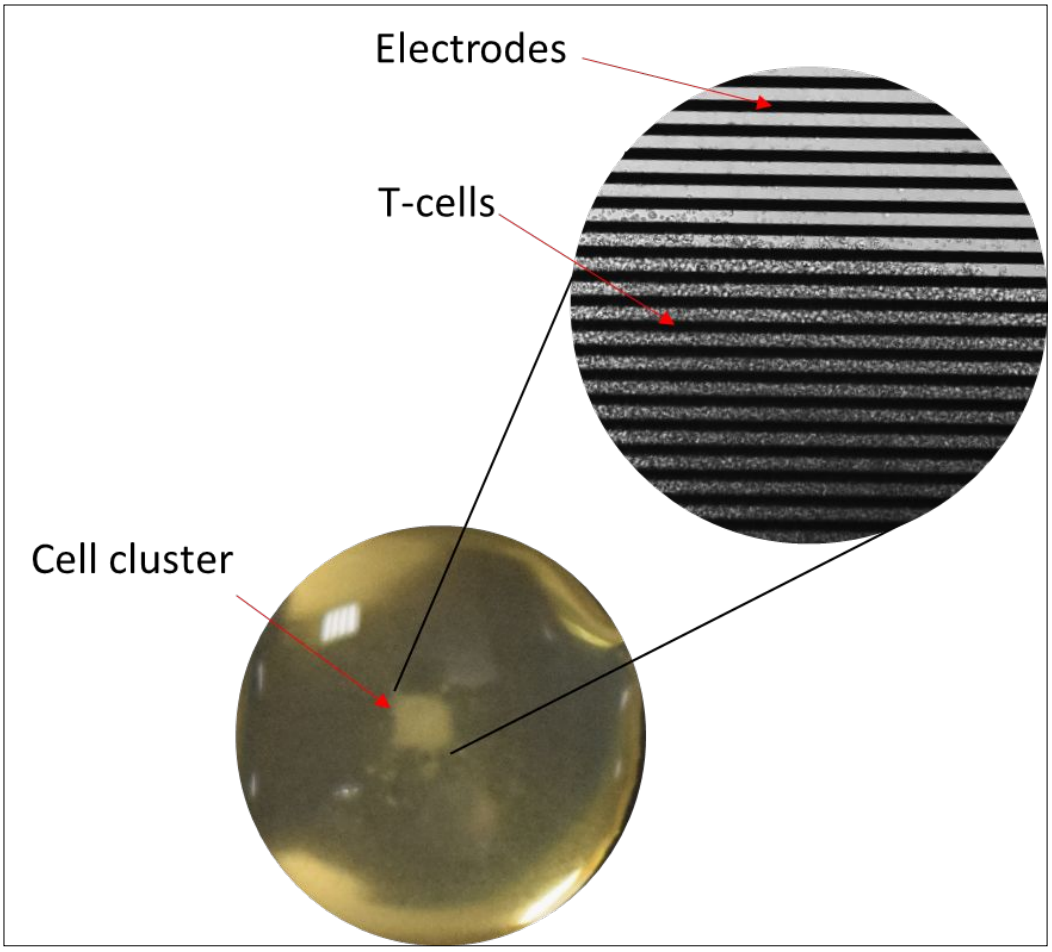


Figure S2: Central aggregate formation of T-cell suspension in buffer. The zoomed inset shows the inverted microscopic image of T-cells forming a multilayered cluster at the center of droplet.